Vol 17 No 4, April 2008
1674-1056/2008/17(04)/1475-05

Chinese Physics B

© 2008 Chin. Phys. Soc.
and IOP Publishing Ltd

Particle-in-Cell/Monte Carlo Collision simulation of planar DC magnetron sputtering*

Zhao Hua-Yu(赵华玉) and Mu Zong-Xin(牟宗信)†

State Key Laboratory of Materials Modification by Laser, Ion and Electron Beams, School of Physics and Optoelectronic Technology, Dalian University of Technology, Dalian 116024, *China*

(Received 5 April 2007; revised manuscript received 21 August 2007)

In this paper a numerical simulation of a planar DC magnetron discharge is performed with the Particle-in-Cell/Monte Carlo Collision (PIC/MCC) method. The magnetic field used in the simulation is calculated with finite element method according to experimental configuration. The simulation is carried out under the condition of gas pressure of 0.665 Pa and voltage magnitude of 400V. Typical results such as the potential distribution, charged particle densities, the discharge current density and ion flux onto the target are calculated. The erosion profile from the simulation is compared with the experimental data. The maximum erosion position corresponds to the place where the magnetic field lines are parallel to the target surface.

Keywords: magnetron sputtering, PIC/MCC, sputtering yield
PACC: 8115C, 7115P, 5275R

1. Introduction

Planar magnetron sputtering device is extensively used as a sputtering source for thin-film deposition.[1,2] In the magnetron discharge, electrons are well confined in the region where magnetic field line is parallel to the cathode surface, leading to high ionization of the background gas. Ions produced in this region are accelerated by the cathode sheath towards the target. Bombardments of the cathode by these ions consequently cause the desired target sputtering as well as the emission of secondary electrons that sustain the discharge.

In the last decades, the characteristics of magnetron discharge have been intensively studied. Various designed magnetron configurations and the basic physical principles involved are given in Refs.[3,4]. The work on axial optical emission distribution and the radial current distribution of the planar magnetron discharge,[5,6] established the basis of numerical analysis for magnetron plasma.[7] Various fluid[8,9] and kinetic[10,11] models have been employed on planar magnetrons. As the fluid model is not valid at low gas pressure when the mean free path of electrons strongly exceeds the characteristic length of the discharge, the fully kinetic and self consistent PIC/MCC (particle-in-cell/Monte Carlo Collision)[12] model is often used when the pressure is lower than 1.33 Pa. The PIC/MCC method is the most powerful computational technique for the planar magnetrons at all operational conditions. The price for that is the long computational time.[13] Recently, the hybrid model[14,15] is used to reduce computation cost.

Due to the certain configuration of planar magnetron, the magnetic field above the target surface is quite complex and the erosion of the target is non-uniform. The erosion uniformity of the target is a major problem which limits the target utilization. It is of practical use to investigate the influence of magnetic field on the target erosion and the effective way is to use a computer model.

This paper presents a two-dimensional (2D) PIC/MCC model of DC planar magnetron. It is organized as follows. In Section 2, the description of the model is presented. The numerical results and discussion are given in Section 3. Finally we summarize the work in Section 4.

2. Description of the model

The schematic diagram of the planar magnetron used in present simulation is shown in Fig.1. It is cylindrical symmetry towards the axis r=0, the dis-

*Project supported by the National Science Found for Distinguished Young Scholars of China (Grant No 50407015).
†Corresponding author. E-mail: mzongxin@dlut.edu.cn

tance between the sputtering cathode and the opposite grounded anode is 3 cm, the cathode is a copper disk with radius r=4.5 cm. The magnetic field is created by permanent magnets located under the cathode and the field structure is unbalanced. The length of the plotted vectors is proportional to the magnetic field strength B. The magnetic field is calculated with finite element method (FEM) software ANSYS according to experimental configuration. The calculated field data is compared with the experimentally measured one in Fig.2. The zone where the magnetic field lines are parallel to the cathode (B_z=0), is at radius r_0=2.5 cm.

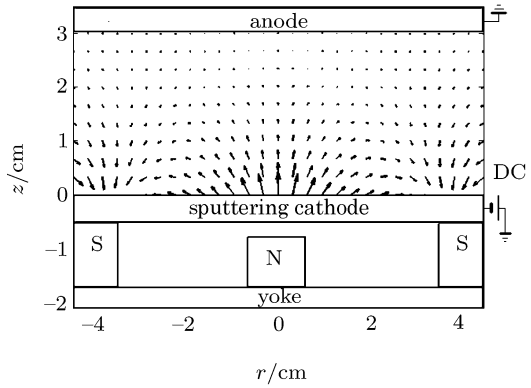


Fig.1. The schematic diagram of the planar magnetron.

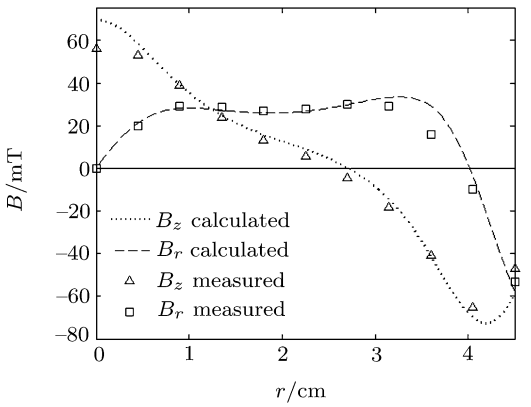


Fig.2. Magnetic field above the target surface.

In PIC simulation, the fields or the energy and velocity distributions can be obtained self-consistently without any assumptions. Collisions can be statistically represented in PIC simulations by coupling PIC methods with Monte Carlo collisions. In this model, the 2D Object-Oriented PIC simulation code XOOPIC[16] is adopted. The magnetic field is assumed to be unaffected by the spatial distribution of the charged particles. The applied DC voltage on the cathode is –400V. The background gas Ar is at temperature 300K, and the gas pressure is 0.665 Pa. The secondary electron emission coefficient γ is 0.1.

3. Results and discussion

3.1. Electrical potential distribution

The plasma potential $\phi(r, z)$ is entirely negative near the cathode. In the far region from the cathode, the plasma potential is weakly positive. The confined region, characterized by a higher plasma potential in Fig.3, is about from the cathode to the negative glow edge. This region corresponds to the place with crossed electric and magnetic fields. As the electric field is axially dominant in the cathode fall, the highest confined region in front of the cathode corresponds to the place where B_z=0.

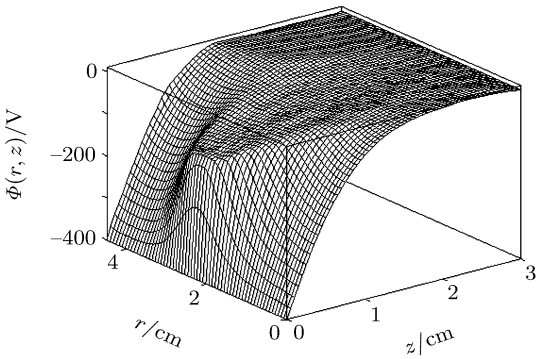


Fig.3. Distribution of the electric potential.

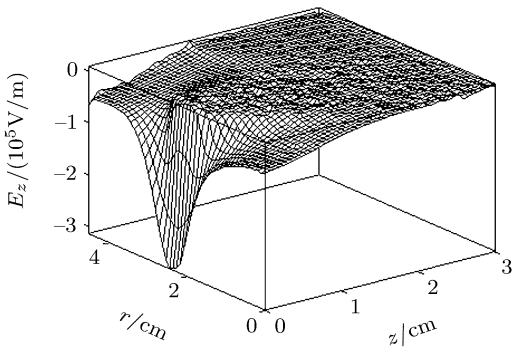


Fig.4. Axial electric field distribution.

The cathode fall thickness is not radially uniform. The minimum cathode fall thickness appears near radius r_0=2.5 cm, not exceeding 0.2 cm (Fig.4). The axial electric field $E_z = -\partial\phi/\partial z$ in the cathode fall is significantly high which reaches up to 3×10^5 V/m.

3.2. Densities of electron and Ar^+

The calculated electron density distribution in Fig.5 has a maximum value of $5\times10^{10}\mathrm{cm}^{-3}$ near the point (r_0, z_0), where z_0=0.24 cm. The calculated ion density distribution shown in Fig.6 has the same profile as the electron density except in the cathode fall. The density peak coincides with the highest confined region. In the confined region, electrons are accelerated by cathode sheath to high-energy states, more inelastic collisions occur and a greater number of slow electrons appear.

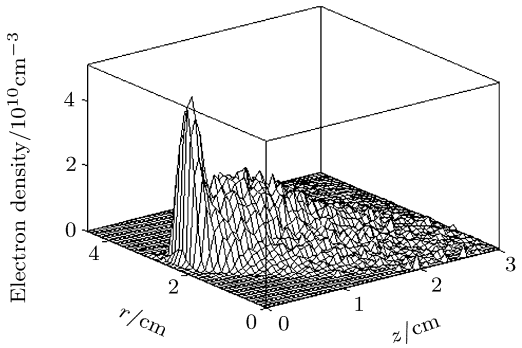


Fig.5. Calculated electron density distribution.

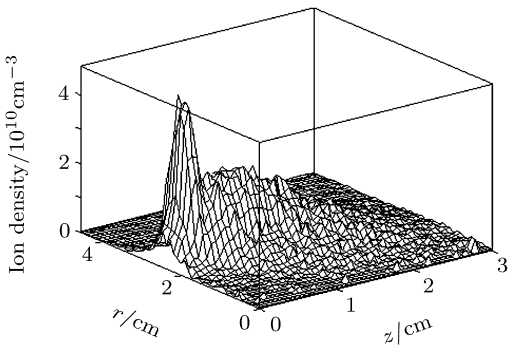


Fig.6. Calculated Ar^+ density distribution.

Under the influence of the crossed electric and magnetic fields, the drift along the direction of $E \times B$ makes electrons move more slowly in the z direction, trapping the high-energy electrons and consequently leads to an increase in inelastic collisions. The enhanced collisions cause more energy loss and create more ions. Electrons are well confined in this region while ions are not. When the ions start to escape, the charge separation creates an inwardly directed electric field to impede the ion loss. This is why the ion has the same density distribution as the electron.

3.3. Sputtering at cathode surface

As the target erosion is strongly correlated to the ion flux onto the target surface, the energy of incident ions onto the target is important to obtain the exact sputtering rate. The spatial and energy distribution function (IEDF) of argon ions on boundary cathode $F(r, E)$ is shown in Fig.7. E is the energy of the incident ion and the majority of the ions are in the energy range above 300 eV, about 80% of the applied voltage.

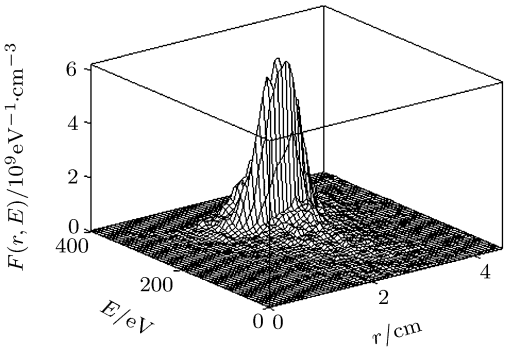


Fig.7. The IEDF of incident ions on boundary cathode.

The ion current density at cathode surface $J_i(r)$, shown in Fig.8, is calculated by

$$J_i(r) = e \int F(r, E)v(E)\mathrm{d}E, \qquad (1)$$

where the ion velocity $v(E)$, converted by $v = \sqrt{2E/m_{\mathrm{ion}}}$, is the function of E. The ion contribution to the discharge current can be integrated by $I_i = 2\pi \int J_i(r)r\mathrm{d}r$. With the second electron emission coefficient γ, we can estimate that the whole discharge current is $I = I_i(1 + \gamma)$=1.6 A. When the discharge voltage is –400V, the calculated current value coincides with the $I - V$ characteristics of our magnetron setup.[17]

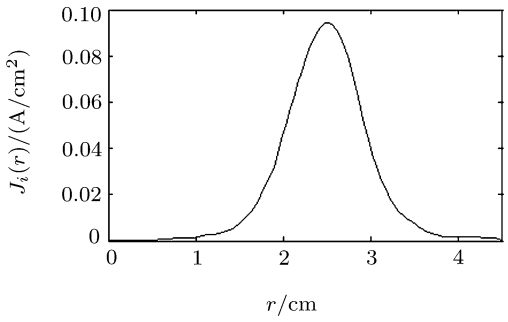


Fig.8. The ion current density at cathode surface.

The ion-induced sputtering flux depends on the ion flux and the corresponding impact energy. The

sputtering flux is obtained by

$$\Gamma(r) = \int F(r,E)v(E)Y(E)\mathrm{d}E, \qquad (2)$$

where $Y(E)$ is the sputtering yield, it can be calculated by Yamamura's formula[18]

$$Y(E) = \frac{0.42\alpha_s Q_s S_\mathrm{n}(E)}{U_0\left[1+0.35U_0 S_\mathrm{e}(\varepsilon)\right]}\left(1-\sqrt{\frac{E_\mathrm{th}}{E}}\right)^{2.8}. \qquad (3)$$

Here we do not consider the effect of angular distribution of the incident ion, α_s and Q_s are experimental parameters, U_0 is sublimation energy of cathode material, E_th is threshold energy. As for $\mathrm{Cu/Ar^+}$ sputtering, the values of these parameters are listed in Table 1. ε is the reduced energy, $S_\mathrm{e}(\varepsilon)$ is the reduced electron stopping cross section and $S_\mathrm{n}(E)$ is the nuclear stopping cross section.[19]

Table 1. Parameter value of $\mathrm{Cu/Ar^+}$ sputtering.

parameter	α_s	Q_s	U_0/eV	E_th/eV
value	0.26	1.27	3.49	13.28

Sputtered particles from the target are created by incident ions bombardments. In Fig.9, the peak radial position of the ion flux coincides with the sputtering flux at radius r_0=2.5 cm, this is the same position of peak plasma density. As a result, the maximum erosion should occur at this place.

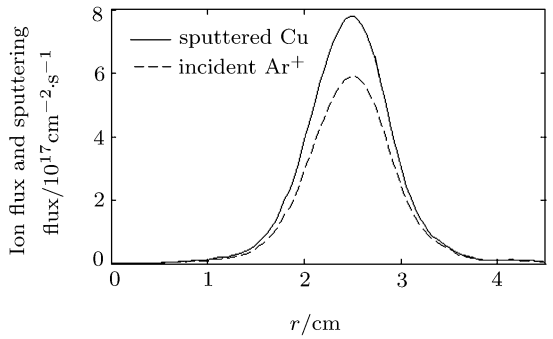


Fig.9. Ion flux and sputtering flux of Cu atom at cathode surface.

The erosion rate of target material can be used to estimate the target life. It describes the erosion depth within certain time and it can be obtained by

$$R(r) = \frac{1}{\rho}\int F(r,E)Y(E)v(E)\mathrm{d}E, \qquad (4)$$

where ρ is the atomic number density of target material. The evolution of the erosion profile of copper target at different time obtained by erosion rate is shown in Fig.10. The maximum erosion rate is about 0.5 mm per hour. The erosion shape measured from a copper target sputtered at the same condition is also given.

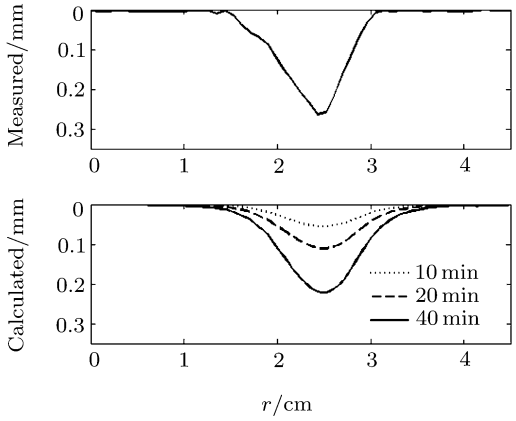


Fig.10. Measured and calculated erosion profile.

The calculated erosion profile is not exactly consistent with the measured one because the latter is a little narrower in the erosion centre. The difference may be that the contribution of fast neutrals is not taken into account in the model. The fast neutrals are caused in the ion-neutral charge change collision process when the ions are accelerated to the cathode surface, so the sputtering caused by fast neutrals is proportional to ion flux. The contribution of fast neutrals is enhancing the erosion at the crater centre. Another reason is due to the real magnetic field configuration does not exactly coincide with the calculated one (Fig.2).

4. Summary

A numerical model for simulation of planar DC magnetron sputtering with PIC/MCC method has been presented. The plasma potential, charged particle densities and ion flux at the cathode surface are obtained. To check the numerical model, the calculated discharge current and the target erosion profile is compared with experiment. The maximum erosion position corresponds to the place where the magnetic field lines are parallel to the target surface. The calculated erosion rate can be used to estimate a target life and utilization of target material under certain magnetic field configuration.

The magnetic field used in the model is calculated with FEM software. With this computer-aided approach, various magnet geometries can be implemented in the model to determine the optimum geometry for magnetron designs. This can significantly reduce experimental efforts. In our future work, the effect of different magnetic field on the target erosion will be discussed.

References

[1] Yang W B, Fan S H, Ma P N, Zhang G L Zhang S Z and Du J 2005 *Acta Phys. Sin.* **54** 4944 (in Chinese)

[2] Li Y P, Liu Z T, Zhao H L, Liu W T and Yan F 2007 *Acta Phys. Sin.* **56** 2937 (in Chinese)

[3] Window B 1995 *Surf. Coat. Tech.* **71** 93

[4] Kelly P J and Arnell R D 2000 *Vacuum* **56** 159

[5] Gu L and Lieberman M A 1988 *J. Vac.Sci. Technol* A **6** 2960

[6] Wendit A E, Lieberman M A and Meuth H 1988 *J. Vac. Sci. Technol* A **6** 1827

[7] Kwon U H, Choi S H, Park Y H and Lee W J 2005 *Thin Solid Films* **475** 17

[8] Bradley J W, Arnell R D and Armour D G 1997 *Surf. Coat. Tech.* **97** 538

[9] Costin C, Marques L, Popa G and Gousset G 2005 *Plasma Sources Sci. Technol.* **14** 168

[10] Shon C H and Lee J K 2002 *Appl. Surf. Sci.* **192** 258

[11] Kondo S and Nanbu K 2001 *J. Vac. Sci. Technol.* A **19** 830

[12] Birdsall C K and Langdon A B 1985 *Plasma Physics via Computer Simulations* (New York: McGraw-Hill)

[13] Kolev I and Bogaerts A 2004 *Contrib. Plasma Phys.* **44** 582

[14] Hagelaar G J M, Bareilles J, Garrigues L and Beouf J P 2003 *J. Appl. Phys.* **93** 67

[15] Yagisawa T and Makabe T 2006 *J. Vac. Sci. Technol.* A **24** 908

[16] Verboncoeur J P, Langdon A B and Gladd N T 1995 *Comput. Phys. Comm.* **87** 199

[17] Mu Z X, Li G Q, Che D L, Huang K Y and Liu C 2004 *Acta Phys. Sin.* **53** 1994 (in Chinese)

[18] Matsunami N, Yamamura Y, Itikawa Y, Itoh N, Kazumata Y, Miyagawa S, Morita K, Shimizu R and Tawara H 1984 *Atom. Data Nucl. Data Tables* **31** 1

[19] Yamamura Y and Tawara H 1996 *Atom. Data Nucl. Data Tables* **62** 149